Coupled Systems Mechanics, *Vol. 11, No. 3 (2022) 233-257*
https://doi.org/10.12989/csm.2022.11.3.233

A comparative study between trapezoidal combined footings and T-shaped combined footings

Marylú García-Galván[a], Arnulfo Luévanos-Rojas*, Sandra López-Chavarría[b], Manuel Medina-Elizondo[c] and José Benito Rivera-Mendoza[d]

Institute of Multidisciplinary Researches, Autonomous University of Coahuila, Blvd. Revolución No, 151 Ote, CP 27000, Torreón, Coahuila, México

(Received August 12, 2021, Revised December 31, 2021, Accepted January 6, 2022)

Abstract. This work presents a comparative study between two different models: trapezoidal and T-shaped combined footings. The comparative study between trapezoidal and T-shaped combined footings presented in this paper generates results that have an unparalleled accuracy for all foundation engineering problems. The main part of this research is to obtain the optimal area, reinforcing steel, and thickness of the trapezoidal and T-shaped combined footings using the new models. The comparison is made for two trapezoidal combined footings and two T-shaped combined footings of reinforced concrete subjected to the same load. The main findings are: the model for trapezoidal combined footings can be used for rectangular and triangular, and the T-shaped combined footings can be used for rectangular. The structure of the paper is as follows first a very complete state of the art with extensive references that describes the methodology used for the different models clearly, presents different numerical examples, results and at the end conclusions.

Keywords: bending shear; design; moments; optimal area; punching shear; T-shaped combined footings; trapezoidal combined footings

1. Introduction

The main feature of the footings or foundations is to transmit the load on the ground. The most suitable type of footing is chosen depending of the depth at which the ground resistance layer is localized to support the structure, the ground condition and the type of structure that must be supported. Foundations are divided into shallow and deep, these account with differences important: in geometry function, the soil behavior, its construction systems, and its structural functionality type (Luévanos-Rojas 2014, 2015b, 2016).

Shallow foundations may be isolated footings (a column), combined footings (two or more columns), strip footings (walls), and rafts or foundation slabs (entire building). The isolated footings

*Corresponding author, Ph.D., E-mail: arnulfol_2007@hotmail.com
[a]Ph.D., E-mail: marylugarciagalvan@live.com.mx
[b]Ph.D., E-mail: sandylopez5@hotmail.com
[c]Ph.D., E-mail: drmanuelmedina@yahoo.com.mx
[d]Ph.D., E-mail: benitoriveramendoza@hotmail.com

http://www.techno-press.org/?journal=csm&subpage=8 ISSN: 2234-2184 (Print), 2234-2192 (Online)

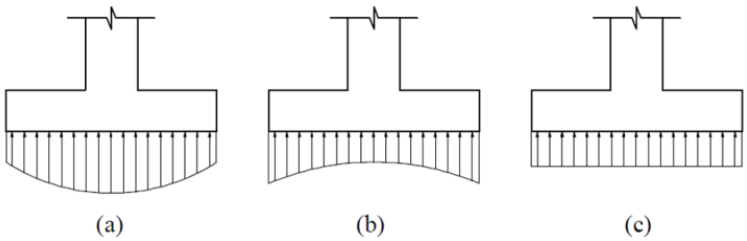

Fig. 1 Pressure distribution diagram; (a) Sandy soils (granular soils); (b) Clayey soils (cohesive soils); (c) Distribution simplified

are classified in square, rectangular, and circular. The combined footings are divided into rectangular, trapezoidal, and T-shaped (Luévanos-Rojas 2015b).

Designs of shallow foundations according to the application of the loads are classified in: 1) Footings with concentric load; 2) Footings with uniaxial bending; 3) Footings with biaxial bending (Luévanos-Rojas 2015b).

The soil pressure under a footing is distributed in accordance with the soil type, the soil relative rigidity and the foundation, and the depth of the contact between foundation and soil. Fig. 1(a) shows the pressure distribution diagram for the footing resting on sandy soils (granular soils). Fig. 1(b) presents the pressure distribution diagram for the footing resting on clayey soils (cohesive soils). Thus, it is assumed for simplicity that the footing is a perfectly rigid body, the soil is behaving elastically and the distributions of the stress and the strain are linear in the soil below the base of the footing. Therefore, the proposed design assumes that the soil pressure is distributed linearly. The distribution of soil pressure is uniform, if the footing centroid coincides with the resultant force of the loads applied on the footing (see Fig. 1(c)) (Luévanos-Rojas 2014, 2015b, Luévanos-Rojas *et al.* 2017b).

Practice construction of a combined footing can be used for more of a column due to: 1) If the columns are located very close to each other (for example, on elevators and escalators); 2) If the size of the footings can be restricted by some property line. If a column located in the footing edge generates an eccentricity on the footing, but, the footing can be attached to the footing of an inner column, and as result a combined footing is obtained.

The traditional model for the design of combined footings by rigid method considers the following (Luévanos-Rojas *et al*. 2017b): 1) The footing or foundation slab is infinitely rigid, and therefore, the deflection of the footing or foundation slab is not influenced in the pressure distribution; 2) The ground pressure distribution must be in straight line or a plane surface such way that the ground pressure centroid must located in the action line of the resultant force (longitudinal axis) of all the loads that act on foundations; 3) The minimum stress is limited to zero, because the ground cannot to support tensile stresses; 4) The maximum stress is limited to the soil allowable load capacity.

Main works of various researchers in recent years on the foundation structures or structural footings are: Guler and Celep (2005) developed the system of plate-column of rectangular shape on the Winkler foundation with tension-less under static and dynamic loads. Wang and Kulhawy (2008) developed the economic design optimization of foundations. Chen *et al*. (2011) presented a study on elastic foundations of nonlinear vibration for hybrid composite plates. Smith-Pardo (2011) showed the framework based on the performance for soil and structure systems by means of foundation models simplified rocking. Shahin and Cheung (2011) proposed the bearing capacity for strip

footings by means of stochastic design charts. Khajehzadeh *et al*. (2012) studied the optimal design for shallow foundations by means the gravitational search algorithm. Rad (2012) investigated elastic foundations with compound loads and gradient thickness to evaluate the static response for a circular plate of 2-D functionally graded. Maheshwari and Khatri (2012) showed the geosynthetic layer inclusion influence on combined footings response on earth beds reinforced with a stone column. Orbanich *et al*. (2012) investigated the concrete foundation beams on the strengthening and repair with fiber composite materials. Mohamed *et al*. (2013) studied the generalized equation of Schmertmann for shallow footings using saturated and unsaturated sands to obtain the settlement. Orbanich and Ortega (2013) analyzed the plates of elastic foundation by means of finite differences method using internal and perimetric reinforcing beams supported on elastic foundations. Luévanos-Rojas (2014) designed the combined footings of rectangular shape to solve the problem of propriety line using a novel model. Hassaan (2014) proposed an optimal design of machinery shallow foundations with sand soils. Luévanos-Rojas (2015a) shows a new mathematical model to find the size of the boundary trapezoidal combined footings, this article presents the equations to obtain the more economical dimensions for trapezoidal combined footings, and it is considered that the resultant force is placed at the gravity center on the "X" axis of the area of the footing, then the moment around the "X" axis does not exist (therefore, optimal area is not presented). Luévanos-Rojas (2015b) proposed a novel model for the design of combined footings with limit on one of its sides of trapezoidal shape; this paper also considers that the resultant force is placed at the gravity center in the direction "Y" of the footing area, i.e., the resultant force is located on the "X" axis. Uncuoğlu *et al*. (2015) estimated the load capacity of the square footings on a layer of sand that overlaps to the clay. Sahoo and Kumar (2015) presented a study for strip and circular shallow foundations on the ultimate bearing capacity by means of the finite elements, limit analysis, and optimization. Luévanos-Rojas (2016) presented a comparison between two novel models for the design of the isolated footings of rectangular and circular type, and the results shown that the circular footings are more economical. Dagdeviren (2016) analyzed the stresses below of the rectangular footings subjected to biaxial bending on an elastic soil. Rezaei *et al*. (2016) studied the thin-walled shallow foundations bearing capacity: an experimental study by means of the artificial intelligence. López-Chavarría *et al*. (2017) showed the optimal dimensioning for the corner combined footings. Luévanos-Rojas *et al*. (2017a) proposed a model optimized for the design of the isolated footings that have rectangular shape taking into account the real soil pressure. Khatri *et al*. (2017) studied the behavior of the pressure and the settlement of skirted footings (square and rectangular) resting on sandy soil. Anil *et al*. (2017) investigated experimentally and analytically the bearing capacities and settlement profiles of six irregularly shaped footings located on sand. Luévanos-Rojas *et al*. (2017b) showed a comparison between two novel models for the design of the combined footings that have trapezoidal and rectangular shape, and the results indicated that the trapezoidal footings are more economical. Mohebkhah (2017) investigated the load capacity for the strip footings on a stone masonry trench in clay. Maheshwari (2017) analyzed the combined footings that rest on an extensible geosynthetic reinforced granular bed on stone column in improved soils. Gandomi and Kashani (2018) used the recent swarm intelligence techniques to estimate the construction minimum cost of the shallow foundation. Hadzalic *et al*. (2018) developed a numerical model for the fluid-structure interaction between structure constructed of porous media and acoustic fluid. Rawat and Mittal (2018) studied the optimal design for reinforced concrete isolated footings with eccentric load. Luévanos-Rojas *et al*. (2018a) presented a new model for T-shaped combined footings to obtain the optimal area of the contact surface on the soil. Luévanos-Rojas *et al*. (2018b) proposed a new model for T-shaped combined footings to obtain the thickness and reinforcing steel area of the

footing. Zhang *et al*. (2019) investigated the bearing behavior of reinforced concrete column isolated footing substructures. Turedi *et al*. (2019) carried out twenty tests in geotechnical laboratory and analyzed numerically by the finite element method to obtain the load-settlement and vertical stress of the ring footings on the loose sand bed. Hadzalic *et al*. (2020) analyzed a 3D lattice model for a thermohydro mechanically coupled discrete beam of a structure constructed by non-isothermal saturated poroplastic medium subjected to mechanical loads and nonstationary heat transfer conditions. Al-Abbas *et al*. (2020) presented an experimental study for elastic deformation under isolated footing. Luat *et al*. (2020) applied the artificial neural networks to predict settlement in shallow foundations resting on sandy soils. Mejia-Nava *et al*. (2021) proposed an alternative to the Raleigh equation to obtain the contributions of damping effects of concrete structures by computational methods through multiscale approach. Ibrahimbegovic and Mejia-Nava (2021) developed a damped model to accurately predict the vibration amplitude reduction for any size of structure of multi-scale analysis in a framework.

Thus, there is not paper on the topic with the level of current knowledge on a comparative study between trapezoidal combined footings and T-shaped combined footings.

This article presents a comparative study between trapezoidal and T-shaped combined footings, these models consider that soil support layers are elastic and the rigid footing, which comply with the biaxial bending equation, i.e., the pressure diagram presents a linear variation. The methodology of the two footings is presented in two parts: the first is the optimal dimension to obtain the sides of the footing, and the second is the design to obtain the thickness and reinforcing steel area of the footing. The model normally used considers that the resultant force is placed at the center of gravity in the "Y" direction of the footing area, i.e., the resultant force is located on the "X" axis (transverse axis). This investigation considers that the footing contact area with the soil is subject to compression on entire base. The comparison is made for two trapezoidal combined footings and two T-shaped combined footings of reinforced concrete subjected to the same load. The first case considers a restricted side (a property line), and the second case takes into account two opposite restricted sides (two property lines).

2. Methodology

2.1 General principles for footings

The two models consider that the footing contact area with the soil is subject to compression on entire base, i.e., the resultant force of all axial loads and moments is located in the central core of the footing.

The equations for the trapezoidal and T-shaped combined footings subjected to a vertical axial load and two orthogonal moments due to each column are presented in a simplified way, and the effects of lateral loads that could occur in the footings are considered at the moments.

The critical sections for footing that supports a reinforced concrete column according to the construction code are:: 1) For the moment occurs on the column face; 2) For the bending shear occurs at a distance "d" from the column face; 3) For the punching shear is located on "b_o" (critical section perimeter that is locate at a distance "d/2" from the column face in both direction) (ACI 318-14).

The general equation to obtain the stress anywhere under biaxial bending is (Luévanos-Rojas 2014, 2015a, b; Luévanos-Rojas *et al.* 2017a, b)

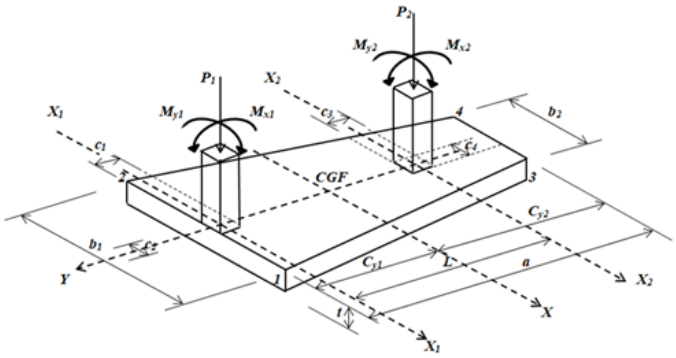

Fig. 2 Trapezoidal combined footing

$$\sigma = \frac{P}{A} + \frac{M_x y}{I_x} + \frac{M_y x}{I_y} \tag{1}$$

where: σ=stress generated by the ground anywhere of the footing (soil pressure), A=area in plant of the footing (contact surface on the soil), P=concentric load on the footing, M_x=moment around the "X" axis, M_y=moment around the "Y" axis, x=distance measured from the "Y" axis in the direction "X" to the point in study, y=distance measured from the "X" axis in direction "Y" to the point in study, I_y=moment of inertia around the "Y" axis and I_x=moment of inertia around the "X" axis. The moments (M_x and M_y) in the clockwise direction are positive.

2.2 Trapezoidal combined footings

Fig. 2 shows a trapezoidal combined footing that supports two rectangular columns of different dimensions, a column located on the property line and another column located on the inside of the construction under an concentric load and moments around of the "X" and "Y" axes (biaxial bending) due to each column.

The stresses in each vertex of the trapezoidal combined footing by Eq. (1) are obtained

$$\sigma_1 = \frac{R}{A} + \frac{M_{xT} C_{y1}}{I_x} + \frac{M_{yT} b_1}{2I_y} \tag{2}$$

$$\sigma_2 = \frac{R}{A} + \frac{M_{xT} C_{y1}}{I_x} - \frac{M_{yT} b_1}{2I_y} \tag{3}$$

$$\sigma_3 = \frac{R}{A} - \frac{M_{xT} C_{y2}}{I_x} + \frac{M_{yT} b_2}{2I_y} \tag{4}$$

$$\sigma_4 = \frac{R}{A} - \frac{M_{xT} C_{y2}}{I_x} - \frac{M_{yT} b_2}{2I_y} \tag{5}$$

where: R=resultant force of the loads P_1 and P_2, M_{xT}=resultant moment about the X axis, M_{yT}=resultant moment about the Y axis, and σ_1, σ_2, σ_3, σ_4=stresses generated by the ground on the footing as seen in Fig. 2.

The mechanical elements that act on the footing are obtained as follows

$$R = P_1 + P_2 \tag{6}$$

$$M_{xT} = M_{x1} + M_{x2} + P_1\left(C_{y1} - \frac{c_1}{2}\right) - P_2\left(L + \frac{c_1}{2} - C_{y1}\right) \tag{7}$$

$$M_{yT} = M_{y1} + M_{y2} \tag{8}$$

The geometric properties of the trapezoidal section of the footing are

$$A = \frac{a(b_1 + b_2)}{2} \tag{9}$$

$$C_{y1} = \frac{a(b_1 + 2b_2)}{3(b_1 + b_2)} \tag{10}$$

$$C_{y2} = \frac{a(2b_1 + b_2)}{3(b_1 + b_2)} \tag{11}$$

$$I_x = \frac{a^3\left(b_1{}^2 + 4b_1b_2 + b_2{}^2\right)}{36(b_1 + b_2)} \tag{12}$$

$$I_y = \frac{a(b_1 + b_2)\left(b_1{}^2 + b_2{}^2\right)}{48} \tag{13}$$

The geometry conditions are

$$\frac{c_1}{2} + L + \frac{c_3}{2} \leq a \tag{14}$$

2.2.1 Optimal dimensions

The objective function to minimize the contact surface of the footing "A_t" is

$$A_t = \frac{a(b_1 + b_2)}{2} \tag{15}$$

Substituting Eqs. (9)-(13) into Eqs. (2)-(5) to obtain the stresses of the trapezoidal combined footing in each vertex (footing corners), and substituting the Eq. (10) into Eq. (7) to obtain M_{xT} in function of the footing sides, and the generalized constraint functions are obtained

$$R = P_1 + P_2 \tag{16}$$

$$M_{xT} = R\left[\frac{a(b_1 + 2b_2)}{3(b_1 + b_2)} - \frac{c_1}{2}\right] + M_{x1} + M_{x2} - P_2L \tag{17}$$

$$M_{yT} = M_{y1} + M_{y2} \tag{18}$$

$$\sigma_1 = \frac{2R}{a(b_1 + b_2)} + \frac{12M_{xT}(b_1 + 2b_2)}{a^2\left(b_1{}^2 + 4b_1b_2 + b_2{}^2\right)} + \frac{24M_{yT}b_1}{a(b_1 + b_2)\left(b_1{}^2 + b_2{}^2\right)} \tag{19}$$

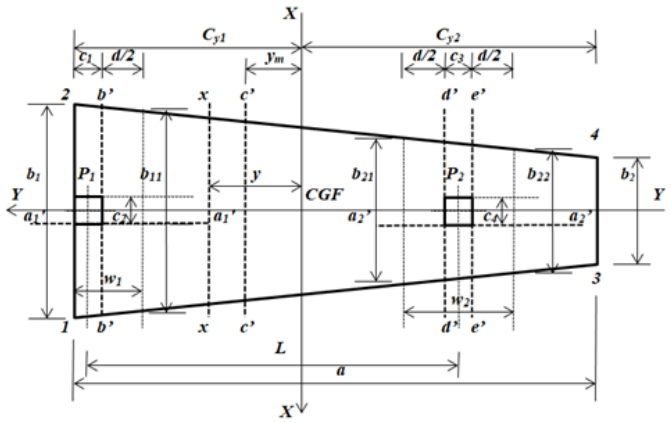

Fig. 3 Critical sections for moments

$$\sigma_2 = \frac{2R}{a(b_1+b_2)} + \frac{12M_{xT}(b_1+2b_2)}{a^2\left({b_1}^2+4b_1b_2+{b_2}^2\right)} - \frac{24M_{yT}b_1}{a(b_1+b_2)\left({b_1}^2+{b_2}^2\right)} \tag{20}$$

$$\sigma_3 = \frac{2R}{a(b_1+b_2)} - \frac{12M_{xT}(2b_1+b_2)}{a^2\left({b_1}^2+4b_1b_2+{b_2}^2\right)} + \frac{24M_{yT}b_2}{a(b_1+b_2)\left({b_1}^2+{b_2}^2\right)} \tag{21}$$

$$\sigma_4 = \frac{2R}{a(b_1+b_2)} - \frac{12M_{xT}(2b_1+b_2)}{a^2\left({b_1}^2+4b_1b_2+{b_2}^2\right)} - \frac{24M_{yT}b_2}{a(b_1+b_2)\left({b_1}^2+{b_2}^2\right)} \tag{22}$$

$$0 \le \begin{Bmatrix}\sigma_1\\ \sigma_2\\ \sigma_3\\ \sigma_4\end{Bmatrix} \le \sigma_{adm} \tag{23}$$

$$\frac{c_1}{2} + L + \frac{c_3}{2} \le a \tag{24}$$

where: σ_{adm}=available permissible load capacity of the soil.

The constant parameters are: P_1, M_{x1}, M_{y1}, P_2, M_{x2}, M_{y2}, c_1, c_2, c_3, c_4, L, σ_{adm}, and the decision variables are: M_{xT}, M_{yT}, R, a, b_1, b_2, A_t, σ_1, σ_2, σ_3, σ_4.

2.2.2 Design

Critical sections for moments occur in the axes: a_1'-a_1', a_2'-a_2', b'-b', c'-c', d'-d' and e'-e' (see Fig. 3).

Equations for the factored moments on the axes a_1'-a_1', a_2'-a_2', b'-b', c'-c', d'-d' and e'-e' are

$$M_{ua_1'} = \frac{P_{u1}[{c_2}^2-(b_1+b_{11})c_2+b_1b_{11}]}{4(b_1+b_{11})} + \frac{3P_{u1}(w_1-c_1)\left({b_1}^2-{b_{11}}^2\right)(b_1-c_2)}{8w_1\left({b_1}^2+4b_1b_{11}+{b_{11}}^2\right)} + \frac{M_{uy1}c_2\left({c_2}^2-{b_1}^2-b_1b_{11}-{b_{11}}^2\right)}{(b_1+b_{11})\left({b_1}^2+{b_{11}}^2\right)} + \frac{M_{uy1}b_1b_{11}}{\left({b_1}^2+{b_{11}}^2\right)} \tag{25}$$

where the analysis width in the section of the a_1'-a_1' axis is: $w_1 = c_1 + d/2$.

$$M_{ua_2'} = \frac{P_{u2}[c_4 - (b_{21} + b_{22})c_4 + b_{21}b_{22}]}{4(b_{21} + b_{22})} + \frac{3P_{u2}(w_2 - c_3)\left({b_{21}}^2 - {b_{22}}^2\right)(b_{21} - c_4)}{8w_2\left({b_{21}}^2 + 4b_{21}b_{22} + {b_{22}}^2\right)} + \frac{M_{uy2}c_4\left({c_4}^2 - {b_{21}}^2 - b_{21}b_{22} - {b_{22}}^2\right)}{(b_{21} + b_{22})\left({b_{21}}^2 + {b_{22}}^2\right)} + \frac{M_{uy2}b_{21}b_{22}}{\left({b_{21}}^2 + {b_{22}}^2\right)} \quad (26)$$

where the analysis width in the section of the a_2'-a_2' axis is: $w_2 = c_3 + d$. The values of P_{u1} and P_{u2} are the factored loads acting on the footing, M_{uy1} and M_{uy2} are the factored moments acting on the footing, w_1 and w_2 are the widths of the analysis surface under the columns in the longitudinal direction ("Y" axis), the values of b_{11}, b_{21} and b_{22} are the widths in the transverse direction, these are: $w_1 = c_1 + d/2;\ w_2 = c_3 + d;\ b_{11} = b_1 - w_1(b_1 - b_2)/a;\ b_{21} = b_1 - (L + c_1/2 - w_2/2)(b_1 - b_2)/a;\ b_{22} = b_1 - (L + c_1/2 + w_2/2)(b_1 - b_2)/a$. If column 2 is located on the limit of the footing, the following must be considered: $w_2 = c_3 + d/2; b_{21} = b_1 - (L + c_1/2 + c_3/2 - w_2)(b_1 - b_2)/a;\ b_{22} = b_2$.

The general equation of factored moments around the X-X axis for the interval: C_{y1}-L-$c_1/2 \leq y \leq C_{y1}$-$c_1/2$.

$$M_{ux} = \frac{M_{uxT}(b_1 - b_2)\left(y^4 - 2C_{y1}y^3 + 2{C_{y1}}^3y - {C_{y1}}^4\right)}{12I_xa} + \frac{M_{uxT}b_1\left(2{C_{y1}}^3 + y^3 - 3{C_{y1}}^2y\right)}{6I_x} + \frac{R_ub_1\left(C_{y1} - y\right)^2}{2A} - \frac{P_{u1}\left(2C_{y1} - c_1 - 2y\right)}{2} + \frac{R_u(b_1 - b_2)\left(y - C_{y1}\right)^3}{6Aa} - M_{ux1} \quad (27)$$

where: M_{uxT} is factored resultant moment around the X-X axis that act on the footing, R_u is the resultant force of the factored loads acting on the footing, M_{ux1} and M_{ux2} are factored moments around the X-X axis that act on the columns 1 and 2. The analysis width in the section of the b'-b' axis is: $b_b = b_1 - c_1(b_1 - b_2)/a$. The analysis width in the section of the c'-c' axis is: $b_c = b_1 - \left(C_{y1} - y_m\right)(b_1 - b_2)/a$ (y_m is distance where the shear force is zero measured from "X" axis). The analysis width in the section of the d'-d' axis is: $b_d = b_1 - (2L + c_1 - c_3)(b_1 - b_2)/2a$.

The general equation of factored moments around the X-X axis for the interval: C_{y1}-$a \leq y \leq C_{y1}$-L-$c_1/2$

$$M_{ux} = \frac{M_{uxT}(b_1 - b_2)\left(y^4 - 2C_{y1}y^3 + 2{C_{y1}}^3y - {C_{y1}}^4\right)}{12I_xa} + \frac{M_{uxT}b_1\left(2{C_{y1}}^3 + y^3 - 3{C_{y1}}^2y\right)}{6I_x} + \frac{R_ub_1\left(C_{y1} - y\right)^2}{2A} - \frac{R_u\left(2C_{y1} - c_1 - 2y\right)}{2} + \frac{R_u(b_1 - b_2)\left(y - C_{y1}\right)^3}{6Aa} + P_{u2}L - M_{ux1} - M_{ux2} \quad (28)$$

where: the analysis width in the section of the e'-e' axis is: $b_e = b_1 - (2L + c_1 + c_3)(b_1 - b_2)/2a$. Substituting "$y$=$C_{y1}$-$c_1$" into Eq. (27) is obtained $M_{ub'}$. Now, Eq. (27) is derived, and it must be equal to zero to obtain the position of the maximum moment "y_m", and substituting "y_m" into Eq. (27) is obtained $M_{uc'}$. Substituting "y=C_{y1}-$c_1/2$-L+$c_3/2$" into Eq. (27) is obtained $M_{ud'}$. Now, substituting "y=C_{y1}-$c_1/2$-L-$c_3/2$" into Eq. (28) is obtained $M_{ue'}$.

Critical sections for bending shear occur in the axes: f_1'-f_1', f_2'-f_2', g'-g', h'-h' and i'-i' (see Fig. 4).

Equations for factored bending shear on the axes f_1'-f_1', f_2'-f_2', g'-g', h'-h' and i'-i' are

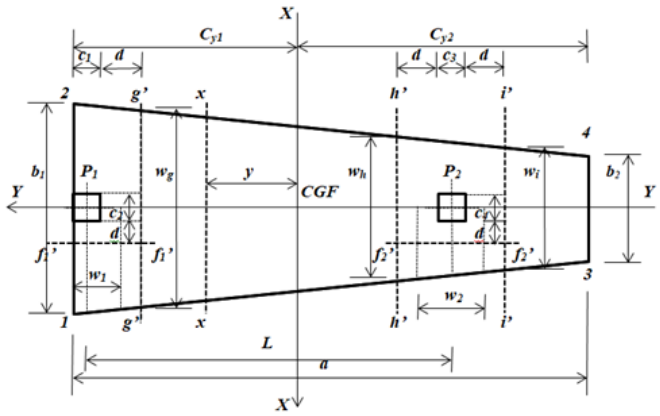

Fig. 4 Critical sections for bending shear

$$V_{uf_1}{}' = \frac{M_{uy1}\left[6(c_2+2d)^2 - 2\left({b_1}^2 + b_1 b_{11} + {b_{11}}^2\right)\right]}{(b_1+b_{11})\left({b_1}^2+{b_{11}}^2\right)} + \frac{P_{u1}(2c_2+4d-b_1-b_{11})}{2(b_1+b_{11})} - \frac{3[2M_{ux1}+P_{u1}(w_1-c_1)]\left({b_1}^2-{b_{11}}^2\right)}{4w_1\left({b_1}^2+4b_1b_{11}+{b_{11}}^2\right)} \tag{29}$$

where the analysis width in the section of the f1'-*f*1' axis is: $b_{f_1} = w_1 = c_1 + d/2$.

$$V_{uf_2}{}' = \frac{M_{uy2}\left[6(c_4+2d)^2 - 2\left({b_{21}}^2 + b_{21}b_{22} + {b_{22}}^2\right)\right]}{(b_{21}+b_{22})\left({b_{21}}^2+{b_{22}}^2\right)} + \frac{P_{u2}(2c_4+4d-b_{21}-b_{22})}{2(b_{21}+b_{22})} - \frac{3[2M_{ux2}+P_{u2}(w_2-c_3)]\left({b_{21}}^2-{b_{22}}^2\right)}{4w_2\left({b_{21}}^2+4b_{21}b_{22}+{b_{22}}^2\right)} \tag{30}$$

where the analysis width in the section of the *f*2'-*f*2' axis is: $b_{f_2} = w_2 = c_3 + d$.

The general equation of the factored shear force at a distance "y" on an axis parallel to X-X axis for the interval: C_{y1}-L-$c_1/2 \leqslant y \leqslant C_{y1}$-$c_1/2$.

$$V_{uy} = P_{u1} - \frac{M_{uxT}(b_1-b_2)\left({C_{y1}}^3-y^3\right)}{3I_x a} - \frac{M_{uxT}\left[ab_1 - C_{y1}(b_1-b_2)\right]\left({C_{y1}}^2-y^2\right)}{2I_x a} - \frac{R_u\left[ab_1 - C_{y1}(b_1-b_2)\right](C_{y1}-y)}{Aa} - \frac{R_u(b_1-b_2)\left({C_{y1}}^2-y^2\right)}{2Aa} \tag{31}$$

where the analysis width in the section of the *g'*-*g'* axis is: $b_g = b_1 - (c_1+d)(b_1-b_2)/a$. The analysis width in the section of the *h*'-*h*' axis is: $b_h = b_1 - (2L + c_1 - c_3 - 2d)(b_1-b_2)/2a$.

The general equation of the factored shear force at a distance "y" on an axis parallel to X-X axis for the interval: C_{y1}-$a \leqslant y \leqslant C_{y1}$-$L$-$c_1/2$.

$$V_{uy} = P_{u1} + P_{u2} - \frac{M_{uxT}(b_1-b_2)\left({C_{y1}}^3-y^3\right)}{3I_x a} - \frac{M_{uxT}\left[ab_1 - C_{y1}(b_1-b_2)\right]\left({C_{y1}}^2-y^2\right)}{2I_x a} - \frac{R_u\left[ab_1 - C_{y1}(b_1-b_2)\right](C_{y1}-y)}{Aa} - \frac{R_u(b_1-b_2)\left({C_{y1}}^2-y^2\right)}{2Aa} \tag{32}$$

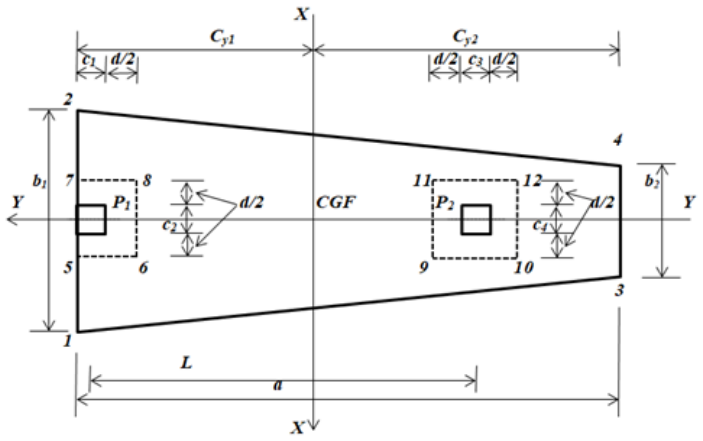

Fig. 5 Critical sections for punching shear

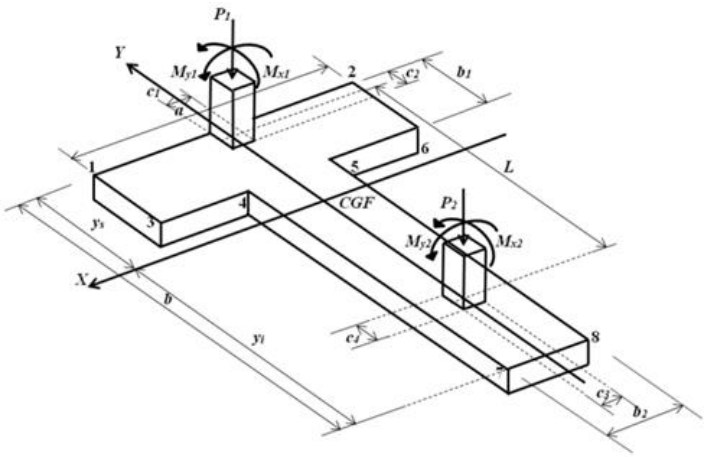

Fig. 6 T-shaped combined footing

where the analysis width in the section of the *i*'-*i*' axis is: $b_i = b_1 - (2L + c_1 + c_3 + 2d)(b_1 - b_2)/2a$.

Substituting "$y=C_{y1}-c_1-d$" into Eq. (31) is obtained $V_{ug'}$. Substituting "$y=C_{y1}-c_1/2-L+c_3/2+d$" into Eq. (31) is obtained $V_{uh'}$. Now, substituting "$y=C_{y1}-c_1/2-L-c_3/2-d$" into Eq. (32) is obtained $V_{ui'}$.

Critical section for punching shear is shown on the formed perimeter by points 5, 6, 7 and 8 for boundary column, and points 9, 10, 11 and 12 for inner column (see Fig. 5).

Equations for factored punching shear for boundary column "V_{up1}" and inner column "V_{up2}" are

$$V_{up1} = P_{u1} - \frac{\left[R_u I_x + M_{uxT} A\left(C_{y1} - c_1/2 - d/4\right)\right](c_2 + d)(c_1 + d/2)}{AI_x} \tag{33}$$

$$V_{up2} = P_{u2} - \frac{\left[R_u I_x + M_{uxT} A\left(C_{y1} - L - c_1/2\right)\right](c_4 + d)(c_3 + d)}{AI_x} \tag{34}$$

If the column 2 is boundary column, then the equation is similar to Eq. (33).

2.3 T-shaped combined footings

Fig. 6 shows a T-shaped combined footing that supports two rectangular columns of different size, a column located on the property line and another column located on the inside of the construction under an concentric load and moments around of the "X" and "Y" axes (biaxial bending) due to each column.

The stresses in each vertex of the T-shaped combined footing by Eq. (1) are obtained

$$\sigma_1 = \frac{R}{A} + \frac{M_{xT} y_s}{I_x} + \frac{M_{yT} a}{2I_y} \tag{35}$$

$$\sigma_2 = \frac{R}{A} + \frac{M_{xT} y_s}{I_x} - \frac{M_{yT} a}{2I_y} \tag{36}$$

$$\sigma_3 = \frac{R}{A} + \frac{M_{xT} (y_s - b_1)}{I_x} + \frac{M_{yT} a}{2I_y} \tag{37}$$

$$\sigma_4 = \frac{R}{A} + \frac{M_{xT} (y_s - b_1)}{I_x} + \frac{M_{yT} b_2}{2I_y} \tag{38}$$

$$\sigma_5 = \frac{R}{A} + \frac{M_{xT} (y_s - b_1)}{I_x} - \frac{M_{yT} b_2}{2I_y} \tag{39}$$

$$\sigma_6 = \frac{R}{A} + \frac{M_{xT} (y_s - b_1)}{I_x} - \frac{M_{yT} a}{2I_y} \tag{40}$$

$$\sigma_7 = \frac{R}{A} - \frac{M_{xT} y_i}{I_x} + \frac{M_{yT} b_2}{2I_y} \tag{41}$$

$$\sigma_8 = \frac{R}{A} - \frac{M_{xT} y_i}{I_x} - \frac{M_{yT} b_2}{2I_y} \tag{42}$$

where: R=resultant force of the loads P_1 and P_2, M_{xT}=resultant moment about the X axis, M_{yT}=resultant moment about the Y axis, and σ_1, σ_2, σ_3, σ_4, σ_5, σ_6, σ_7, σ_8=stresses generated by the ground on the footing as seen in Fig. 6.

The mechanical elements that act on the footing are obtained as follows

$$R = P_1 + P_2 \tag{43}$$

$$M_{xT} = M_{x1} + M_{x2} + P_1 \left(y_s - \frac{c_2}{2} \right) - P_2 \left(L + \frac{c_2}{2} - y_s \right) \tag{44}$$

$$M_{yT} = M_{y1} + M_{y2} \tag{45}$$

The geometric properties of the T-section are

$$A = (a - b_2) b_1 + b b_2 \tag{46}$$

$$y_s = \frac{(a-b_2){b_1}^2 + b^2 b_2}{2[(a-b_2)b_1 + bb_2]} \tag{47}$$

$$y_i = \frac{(2b-b_1)(a-b_2)b_1 + b^2 b_2}{2[(a-b_2)b_1 + bb_2]} \tag{48}$$

$$I_x = \frac{a^2 {b_1}^4 + {b_2}^2(b-b_1)^4 + 2ab_1b_2(b-b_1)\left(2b^2 - bb_1 + {b_1}^2\right)}{12[(a-b_2)b_1 + bb_2]} \tag{49}$$

$$I_y = \frac{b_1 a^3 + (b-b_1){b_2}^3}{12} \tag{50}$$

The geometry conditions are

$$\frac{c_2}{2} + L + \frac{c_4}{2} \leq b \tag{51}$$

2.3.1 Optimal dimensions

The objective function to minimize the total area of the contact surface "A_t" is (Luévanos-Rojas *et al*. 2018a)

$$A_t = (a-b_2)b_1 + bb_2 \tag{52}$$

Substituting Eqs. (46)-(50) into Eqs. (35)-(42) to obtain the stresses of the T-shaped combined footing in each vertex and substituting Eq. (47) into Eq. (44) to obtain M_{xT} in function of the footing sides, and the generalized constraint functions are obtained

$$R = P_1 + P_2 \tag{53}$$

$$M_{xT} = \frac{R\left[(a-b_2){b_1}^2 + b^2 b_2\right]}{2[(a-b_2)b_1 + bb_2]} + M_{x1} + M_{x2} - \frac{Rc_2}{2} - P_2 L \tag{54}$$

$$M_{yT} = M_{y1} + M_{y2} \tag{55}$$

$$\sigma_1 = \frac{6M_{xT}\left[(a-b_2){b_1}^2 + b^2 b_2\right]}{a^2 {b_1}^4 + 2ab_1b_2(b-b_1)\left(2b^2 - bb_1 + {b_1}^2\right) + {b_2}^2(b-b_1)^4} + \frac{6M_{yT}a}{b_1 a^3 + (b-b_1){b_2}^3} + \frac{R}{(a-b_2)b_1 + bb_2} \tag{56}$$

$$\sigma_2 = \frac{6M_{xT}\left[(a-b_2){b_1}^2 + b^2 b_2\right]}{a^2 {b_1}^4 + 2ab_1b_2(b-b_1)\left(2b^2 - bb_1 + {b_1}^2\right) + {b_2}^2(b-b_1)^4} - \frac{6M_{yT}a}{b_1 a^3 + (b-b_1){b_2}^3} + \frac{R}{(a-b_2)b_1 + bb_2} \tag{57}$$

$$\sigma_3 = \frac{6M_{xT}\left[(b-b_1)^2 b_2 - a{b_1}^2\right]}{a^2 {b_1}^4 + 2ab_1b_2(b-b_1)\left(2b^2 - bb_1 + {b_1}^2\right) + {b_2}^2(b-b_1)^4} + \frac{6M_{yT}a}{b_1 a^3 + (b-b_1){b_2}^3} + \frac{R}{(a-b_2)b_1 + bb_2} \tag{58}$$

$$\sigma_4 = \frac{6M_{xT}\left[(b-b_1)^2 b_2 - a{b_1}^2\right]}{a^2{b_1}^4 + 2ab_1b_2(b-b_1)\left(2b^2 - bb_1 + {b_1}^2\right) + {b_2}^2(b-b_1)^4} + \frac{6M_{yT}b_2}{b_1a^3 + (b-b_1){b_2}^3} + \frac{R}{(a-b_2)b_1 + bb_2} \tag{59}$$

$$\sigma_5 = \frac{6M_{xT}\left[(b-b_1)^2 b_2 - a{b_1}^2\right]}{a^2{b_1}^4 + 2ab_1b_2(b-b_1)\left(2b^2 - bb_1 + {b_1}^2\right) + {b_2}^2(b-b_1)^4} - \frac{6M_{yT}b_2}{b_1a^3 + (b-b_1){b_2}^3} + \frac{R}{(a-b_2)b_1 + bb_2} \tag{60}$$

$$\sigma_6 = \frac{6M_{xT}\left[(b-b_1)^2 b_2 - a{b_1}^2\right]}{a^2{b_1}^4 + 2ab_1b_2(b-b_1)\left(2b^2 - bb_1 + {b_1}^2\right) + {b_2}^2(b-b_1)^4} - \frac{6M_{yT}a}{b_1a^3 + (b-b_1){b_2}^3} + \frac{R}{(a-b_2)b_1 + bb_2} \tag{61}$$

$$\sigma_7 = -\frac{6M_{xT}[(2b-b_1)(a-b_2)b_1 + b^2b_2]}{a^2{b_1}^4 + 2ab_1b_2(b-b_1)\left(2b^2 - bb_1 + {b_1}^2\right) + {b_2}^2(b-b_1)^4} + \frac{6M_{yT}b_2}{b_1a^3 + (b-b_1){b_2}^3} + \frac{R}{(a-b_2)b_1 + bb_2} \tag{62}$$

$$\sigma_8 = -\frac{6M_{xT}[(2b-b_1)(a-b_2)b_1 + b^2b_2]}{a^2{b_1}^4 + 2ab_1b_2(b-b_1)\left(2b^2 - bb_1 + {b_1}^2\right) + {b_2}^2(b-b_1)^4} - \frac{6M_{yT}b_2}{b_1a^3 + (b-b_1){b_2}^3} + \frac{R}{(a-b_2)b_1 + bb_2} \tag{63}$$

$$0 \leq \begin{Bmatrix}\sigma_1\\ \sigma_2\\ \sigma_3\\ \sigma_4\\ \sigma_5\\ \sigma_6\\ \sigma_7\\ \sigma_8\end{Bmatrix} \leq \sigma_{adm} \tag{64}$$

$$\frac{c_2}{2} + L + \frac{c_4}{2} \leq b \tag{65}$$

where: σ_{adm}=available permissible load capacity of the soil.

The constant parameters are: P_1, M_{x1}, M_{y1}, P_2, M_{x2}, M_{y2}, c_1, c_2, c_3, c_4, L, σ_{adm}, and the decision variables are: M_{xT}, M_{YT}, R, a, b, b_1, b_2, A_t, σ_1, σ_2, σ_3, σ_4, σ_5, σ_6, σ_7, σ_8.

2.3.2 Design

Critical sections for moments occur on the axes: *a*'-*a*', *b*'-*b*', *c*'-*c*', *d*'-*d*', *e*'-*e*', *f*'-*f*' and *g*'-*g*' (see Fig. 7).

Equations for the moments on the axes *a*'-*a*', *b*'-*b*', *c*'-*c*', *d*'-*d*', *e*'-*e*', *f*'-*f*' and *g*'-*g*' are (Luévanos-Rojas *et al*. 2018b)

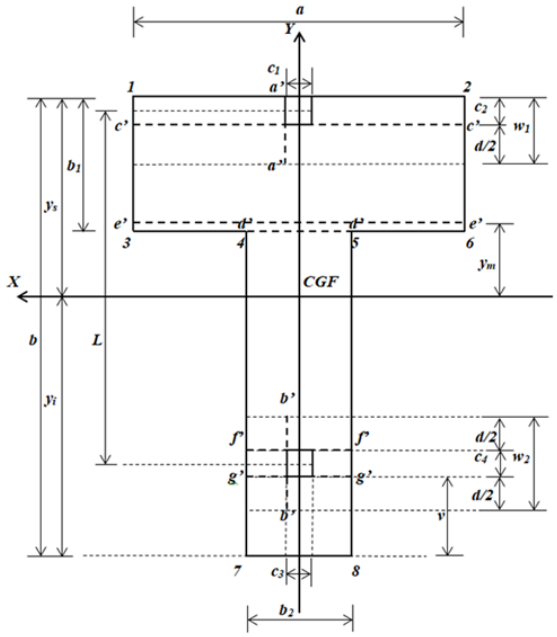

Fig. 7 Critical sections for moments

$$M_{ua'} = \frac{\left[P_{u1}a^2 + 2M_{uy1}(2a + c_1)\right](a - c_1)^2}{8a^3} \tag{66}$$

where the analysis width in the section of the *a*'-*a*' axis is: $w_1 = c_2 + d/2$.

$$M_{ub'} = \frac{\left[P_{u2}{b_2}^2 + 2M_{uy2}(2b_2 + c_3)\right](b_2 - c_3)^2}{8{b_2}^3} \tag{67}$$

where the analysis width in the section of the *b*'-*b*' axis is: $w_2 = c_4 + d$. The values of P_{u1} and P_{u2} are the factored loads acting on the footing, M_{uy1} and M_{uy2} are the factored moments acting on the footing, w_1 and w_2 are the widths of the analysis surface under the columns in the longitudinal direction ("Y" axis).

The general equation of factored moments around the X-X axis for the interval: y_s-$b_1 \leq y \leq y_s$-$c_2/2$.

$$M_{ux} = \frac{M_{uxT}a(2{y_s}^3 + y^3 - 3{y_s}^2 y)}{6I_x} + \frac{R_u a(y_s - y)^2}{2A} - \frac{P_{u1}(2y_s - c_2 - 2y)}{2} - M_{ux1} \tag{68}$$

where the analysis width for this interval is: a.

The general equation of factored moments around the X-X axis for the interval: y_s-$(L + c_2/2) \leq y \leq y_s$-$b_1$.

$$M_{ux} = \frac{M_{uxT}[a{y_s}^2(2y_s - 3y) + b_2 y^3 + (a - b_2)(y_s - b_1)^2(3y - 2y_s + 2b_1)]}{6I_x} + \frac{R_u[ab_1(2y_s - 2y - b_1) + b_2(y - y_s + b_1)^2]}{2A} - \frac{P_{u1}(2y_s - c_2 - 2y)}{2} - M_{ux1} \tag{69}$$

where the analysis width for this interval is: b_2.

The general equation of factored moments around the X-X axis for the interval: y_s-b≤y≤y_s-(L+c_2/2).

$$M_{ux} = \frac{R_u[b_2y^2 + ab_1(2y_s - 2y - b_1) + b_2(y_s - b_1)(y_s - b_1 - 2y)]}{2A} + \frac{M_{uxT}[b_2y^3 + ay_s{}^2(2y_s - 3y) - (a - b_2)(y_s - b_1)^2(2y_s - 2b_1 - 3y)]}{6I_x} - \frac{R_u(2y_s - 2y - 2L - c_2)}{2} - P_{u1}L - M_{ux1} - M_{ux2} \quad (70)$$

where the analysis width for this interval is: b_2.

Substituting "y=y_s-c_2" into Eq. (68) is obtained $M_{uc'}$. Now, Eq. (68) is derived, and it must be equal to zero to find the position of the maximum moment "y_m" (if it falls within the range y_s-b_1≤y≤y_s-c_2/2), and substituting "y_m" into Eq. (68) is obtained $M_{ue'}$. Substituting "y=y_s-b_1" into Equation (68) or Eq. (69) is obtained $M_{ud'}$. Substituting "y=y_s-c_2/2-L+c_4/2" into Eq. (69) is obtained $M_{uf'}$. Now, Eq. (69) is derived, and it must be equal to zero to obtain the position of the maximum moment "y_m" (if it falls within the range y_s-c_2/2-L≤y≤y_s-b_1), and substituting "y_m" into Eq. (69) is obtained $M_{ue'}$. Substituting "y=y_s-c_2/2-L-c_4/2" into Eq. (70) is obtained $M_{ug'}$.

Critical sections for bending shear occur on the axes: h'-h', i'-i'', j'-j', k'-k', l'-l' and m'-m' (see Fig. 8).

Equations for factored bending shear on the axes h'-h', i'-i'', j'-j', k'-k', l'-l' and m'-m' are (Luévanos-Rojas *et al*. 2018b)

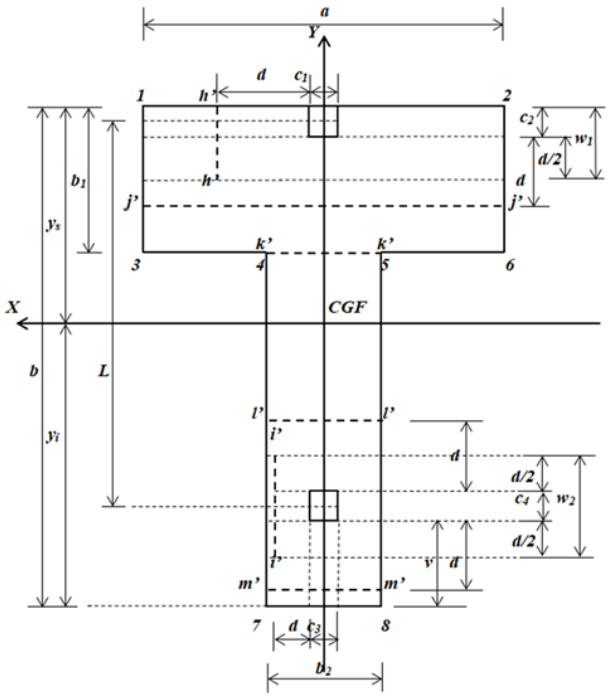

Fig. 8 Critical sections for bending shear

$$V_{uh'} = -\frac{\left[P_{u1}a^2 + 3M_{uy1}(a + c_1 + 2d)\right](a - c_1 - 2d)}{2a^3} \tag{71}$$

where the analysis width in the section of the *h*'-*h*' axis is: $w_1 = c_2 + d/2$.

$$V_{ui'} = -\frac{\left[P_{u2}{b_2}^2 + 3M_{uy2}(b_2 + c_3 + 2d)\right](b_2 - c_3 - 2d)}{2{b_2}^3} \tag{72}$$

where the analysis width in the section of the *i*'-*i*' axis is: $w_2 = c_4 + d$.

The general equation of the factored shear force at a distance "y" on an axis parallel to X-X axis for the interval: y_s-b_1≤y≤y_s-c_2/2.

$$V_{uy} = P_{u1} - \frac{R_u a(y_s - y)}{A} - \frac{M_{uxT}a({y_s}^2 - y^2)}{2I_x} \tag{73}$$

where the analysis width for this interval is: a.

The general equation of the factored shear force at a distance "y" on an axis parallel to X-X axis for the interval: y_s-L-c_2/2≤y≤y_s-b_1

$$V_{uy} = P_{u1} - \frac{R_u[ab_1 + b_2(y_s - y - b_1)]}{A} - \frac{M_{uxT}\{ab_1(2y_s - b_1) + b_2[(y_s - b_1)^2 - y^2]\}}{2I_x} \tag{74}$$

where the analysis width for this interval is: b_2.

The general equation of the factored shear force at a distance "y" on an axis parallel to X-X axis for the interval: y_s-b≤y≤y_s-L-c_2/2.

$$V_{uy} = P_{u1} + P_{u2} - \frac{M_{uxT}\{ab_1(2y_s - b_1) + b_2[(y_s - b_1)^2 - y^2]\}}{2I_x} - \frac{R_u[ab_1 + b_2(y_s - y - b_1)]}{A} \tag{75}$$

where the analysis width for this interval is: b_2.

Substituting "y=y_s-c_2-d" into Eq. (73) (if the j axis falls within the range y_s-b_1≤y≤y_s-c_2/2) or into Eq. (74) (if the j axis falls within the range y_s-L-c_2/2≤y≤y_s-b_1) is obtained $V_{uj'}$. Substituting "y=y_s-b_1" into Eq. (73) or Eq. (74) is obtained $V_{uk'}$. Now, substituting "y=y_s-c_2/2-L+c_4/2+d" into Eq. (74) is obtained V_{ul}. Substituting "y=y_s-c_2/2-L-c_4/2-d" into Eq. (75) is obtained V_{um}.

Critical section for punching shear is shown on the formed perimeter by points 9, 10, 11 and 12 for boundary column, and points 13, 14, 15 and 16 for inner column (see Fig. 9).

Equations for factored punching shear for boundary column "V_{up1}" and inner column "V_{up2}" are (Luévanos-Rojas *et al*. 2018b)

$$V_{up1} = P_{u1} - \frac{[R_u I_x + M_{uxT}A(y_s - c_2/2 - d/4)](c_1 + d)(c_2 + d/2)}{AI_x} \tag{76}$$

$$V_{up2} = P_{u2} - \frac{[R_u I_x + M_{uxT}A(y_s - L - c_2/2)](c_3 + d)(c_4 + d)}{AI_x} \tag{77}$$

If the column 2 is boundary column, then the equation is similar to Eq. (76).

3. Numerical problems

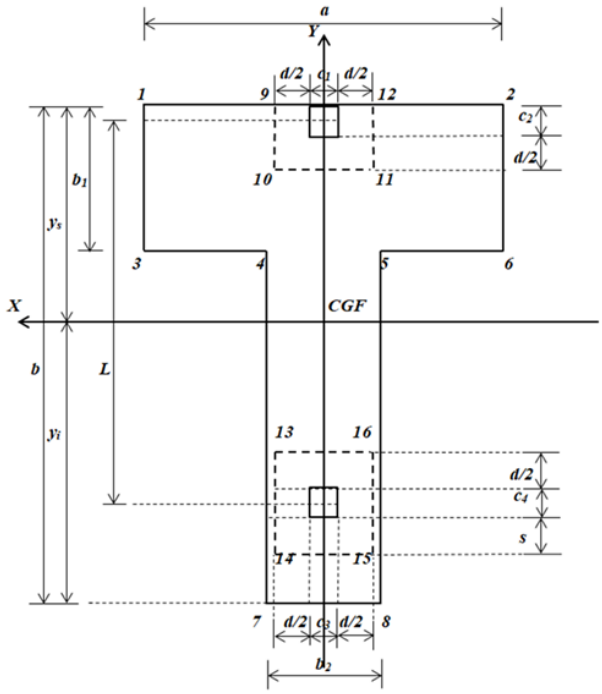

Fig. 9 Critical sections for punching shear

Design of two trapezoidal combined footings and two T-shaped combined footings of reinforced concrete under the same load conditions that supports two square columns (see Figs. 2 and 6). The first case is considered a restricted side (one property line), and the second case is taken into account two opposite restricted sides (two property lines). The data for design are: columns 1 and 2 are of 40×40 cm, L (center-to-center distance between the two columns)=6.00 m, H (depth of the footing)=1.5 m, M_{Dx1} (moment of dead load around the "X-X" axis of the column 1)=80 kN-m, M_{Lx1} (moment of live load around the "X-X" axis of the column 1)=60 kN-m, M_{Dy1} (moment of dead load around the "Y-Y" axis of the column 1) =120 kN-m, M_{Ly1} (moment of live load around the "Y-Y" axis of the column 1) =80 kN-m, P_{D1} (dead load of the column 1) =700 kN, P_{L1} (live load of the column 1) =500 kN, M_{Dx2} (moment of dead load around the "X-X" axis of the column 2) =60 kN-m, M_{Lx2} (moment of live load around the "X-X" axis of the column 2) =40 kN-m, M_{Dy2} (moment of dead load around the "Y-Y" axis of the column 2) =80 kN-m, M_{Ly2} (moment of live load around the "Y-Y" axis of the column 2) =60 kN-m, P_{D2} (dead load of the column 2) =600 kN, P_{L2} (live load of the column 2) =400 kN, f'_c (specified compressive strength of concrete at 28 days) =21 Mpa, f_y (specified yield strength of reinforcement of steel)=420 *Mpa*, q_a (allowable load capacity of the soil) =250 kN/m^2, γ_c (concrete density) =24 kN/m^3, γ_s (soil fill density) =15 kN/m^3, r (coating of the footing) =8 cm.

The available permissible load capacity of the soil "σ_{max}" is obtained as follows, at the allowable load capacity of the soil "q_a" is subtracted from the weight of the footing (γ_c by the thickness of the footing) and the weight of the soil fill (γ_s by the thickness of the filling).

The loads and moments that act on the soil are: P_1=1200 kN, M_{x1}=140 kN-m, M_{y1}=200 kN-m, P_2=1000 kN, M_{x2}=100 kN-m, M_{y2}=140 kN-m.

Table 1 Optimal area of the two cases and the two footings

Concept	Trapezoidal combined footing				T-shaped combined footing			
	Case 1		Case 2		Case 1		Case 2	
$\sigma_{máx}$ (kN/m^2)	217.15		218.50		218.05		217.15	
	First solution	Practical solution	First solution	Practical solution	First solution	Practical solution	First solution	Practical solution
R (kN)	2200.00	2200.00	2200.00	2200.00	2200.00	2200.00	2200.00	2200.00
M_{xT} (kN-m)	− 500.20	− 480.00	426.37	413.59	− 514.49	− 451.86	0.00	− 15.56
M_{yT} (kN-m)	340.00	340.00	340.00	340.00	340.00	340.00	340.00	340.00
Footing sides (m)	a=7.77 b_1=3.52 b_2=0.00	a=7.80 b_1=3.60 b_2=0.00	a=6.40 b_1=4.03 b_2=1.00	a=6.40 b_1=4.10 b_2=1.00	a=5.93 b=7.80 b_1=1.00 b_2=1.00	a=6.00 b=7.90 b_1=1.00 b_2=1.00	a=2.55 b=6.40 b_1=5.00 b_2=1.00	a=2.60 b=6.40 b_1=5.00 b_2=1.00
σ_1 (kN/m^2)	217.15	211.12	218.50	213.96	211.19	210.31	217.15	211.10
σ_2 (kN/m^2)	47.89	49.67	100.01	98.86	98.87	100.48	93.75	92.28
σ_3 (kN/m^2)	217.15	209.29	117.45	116.25	218.05	216.11	217.15	213.03
σ_4 (kN/m^2)	217.15	209.29	88.05	88.18	171.36	170.35	179.66	176.47
σ_5 (kN/m^2)	-	-	-	-	152.42	152.04	131.24	130.77
σ_6 (kN/m^2)	-	-	-	-	105.73	106.28	93.75	94.22
σ_7 (kN/m^2)	-	-	-	-	218.05	210.34	179.66	177.01
σ_8 (kN/m^2)	-	-	-	-	199.11	192.04	131.24	131.32
A_t (m^2)	13.69	14.04	16.10	16.32	12.73	12.90	14.15	14.40

where: $\sigma_{máx}$=Available permissible load capacity of the soil, R=Resultant force, M_{xT}=Resultant moment about the X axis, M_{yT}=Resultant moment about the Y axis, A_t=Minimum area, his bending shear acting on f_2'-f_2' axis is zero, because it falls outside of the support surface of the footing.

Now, the factorized loads and moments are: P_{u1}=1640 kN, M_{ux1}=192 kN-m, M_{uy1}=272 kN-m, P_{u2}=1360 kN, M_{ux2}=136 kN-m, M_{uy2}=192 kN-m.

The properties of the thickness of the trapezoidal combined footing after making several iterations are: t=115 cm, d=107 cm, r=8 cm (case 1), and t=100 cm, d=92 cm, r=8 cm (case 2).

The properties of the thickness of the T-shaped combined footing after making several iterations are: t=105 cm, d=97 cm, r=8 cm (case 1), and t=115 cm, d=107 cm, r=8 cm (case 2).

Table 1 shows the optimal area of the contact surface on the soil for the two cases and the two footings.

Table 2 shows the geometric properties, the factored resultant moments and factored resultant force acting for the two cases and the two footings.

Table 3 shows the factored moments acting on each axis and the section width of the applied moments for the two cases and the two footings.

Table 4 shows the factored bending shear acting on the footing and the bending shear resisted by the concrete for the two cases and the two footings (ACI 318-14).

Table 5 shows the factored punching shear acting on the footing, and three punching shear that

Table 2 Geometric properties and factored resultant mechanical elements for the two cases and the two footings

Concept	Trapezoidal combined footing		T-shaped combined footing	
	Case 1	Case 2	Case 1	Case 2
Geometric properties	A=14.04 m^2, C_{y1}=2.60 m, I_x=47.46 m^4	A=16.32 m^2, C_{y1}=2.55 m, I_x=48.85 m^4	A=12.90 m^2, y_s=2.61 m, I_x=77.95 m^4	A=14.40 m^2, y_s=2.81 m, I_x=40.25 m^4
R_u (kN)	3000.00	3000.00	3000.00	3000.00
M_{uxT} (kN-m)	− 632.00	− 777.10	− 593.63	1.33
M_{uyT} (kN-m)	464	464	464	464

Table 3 Moments acting on each axis for the two cases and the two footings

Trapezoidal combined footing					T-shaped combined footing				
Axis	Case 1		Case 2		Axis	Case 1		Case 2	
	M (kN-m)	w (m)	M (kN-m)	w (m)		M (kN-m)	w (m)	M (kN-m)	w (m)
a_1'-a_1'	695.54	0.935	797.75	0.86	a'-a'	1193.89	0.885	486.48	0.935
a_2'-a_2'	83.17	1.47	163.90	0.86	b'-b'	102.67	1.37	102.67	0.935
b'-b'	− 468.82	3.42	− 473.07	3.90	c'-c'	− 417.43	6.00	− 476.65	2.60
c'-c'	− 2087.91	2.29	− 2212.79	2.68	d'-d'	− 858.34	1.00	− 1291.94	2.60
d'-d'	− 14.39	0.83	− 113.77	1.19	e'-e'	− 1117.83	1.00	− 2346.00	2.60
e'-e'	57.81	0.65	0.00	1.00	f'-f'	348.71	1.00	− 119.35	1.00
					g'-g'	303.71	1.00	0.00	1.00

where: M=Moment, w=Width of the analyzed section.

Table 4 Bending shear on each axis for the two cases and the two footings

Trapezoidal combined footing							T-shaped combined footing						
	Case 1			Case 2				Case 1			Case 2		
Axis	V_f (kN)	$\emptyset_f V_f$ (kN)	w (m)	V_f (kN)	$\emptyset_f V_f$ (kN)	w (m)	Axis	V_f (kN)	$\emptyset_f V_f$ (kN)	w (m)	V_f (kN)	$\emptyset_f V_f$ (kN)	w (m)
f_1'-f_1'	−300.21	662.48	0.935	−453.58	523.92	0.86	h'-h'	−557.86	568.45	0.885	−26.08	662.48	0.935
f_2'-f_2'	0	1041.55	1.47	0	523.92	0.86	i'-i'	0	879.97	1.37	0	662.48	0.935
g'-g'	736.45	2068.92	2.92	874.22	2107.86	3.46	j'-j'	2.59	642.32	1.00	843.49	1842.19	2.60
h'-h'	−870.65	935.27	1.32	−953.28	999.10	1.64	k'-k'	341.06	642.32	1.00	−1068.47	1842.19	2.60
i'-i'	7.04	106.28	0.15	0	0	0	l'-l'	−608.58	642.32	1.00	−1053.89	1842.19	2.60
							m'-m'	143.26	642.32	1.00	0	0	1.00

where: V_f=Bending shear acting on the footing, $\emptyset_f V_f$=Bending shear resisted by the concrete.
Note: * Trapezoidal combined footings: The bending shear acting on f_2'-f_2' (cases 1 and 2) axis and i'-i' (case 2) axis, these values are zero, because it falls outside of the support surface of the footing. ** T-shaped combined footing: The bending shear acting on i'-i' (cases 1 and 2) axis and m'-m' (case 2) axis, these values are zero, because it falls outside of the support surface of the footing. The bending shear acting on k'-k' (case 2) axis is not considered, because it falls within the distance "d" of the inner column. If "d" is reduced to 97 cm, then the analysis width is reduced to 1.00 m, and the bending shear resisted by the concrete is reduced and this does not meet.

Table 5 Punching shear acting on each column for the two cases and the two footings

Column	Trapezoidal combined footing				T-shaped combined footing			
	Case 1		Case 2		Case 1		Case 2	
	V_p (kN)	$Ø_pV_p$ (kN)	V_p (kN)	$Ø_pV_p$ (kN)	V_p (kN)	$Ø_pV_p$ (kN)	V_p (kN)	$Ø_pV_p$ (kN)
1	1385.34	7099.52	1469.61	5555.97	1378.05	6050.62	1353.55	7099.52
	13415.23	4593.81	10017.67	3595.04	11095.23	3915.11	13415.23	4593.81
2	794.68	12498.56	938.54	9649.85	872.20	10559.69	910.05	12498.56
	18874.04	8087.30	14086.60	6244.02	15604.82	6832.74	18874.04	8087.30

where: V_p=Punching shear acting on the footing, $Ø_pV_p$=Punching shear resisted by the concrete.

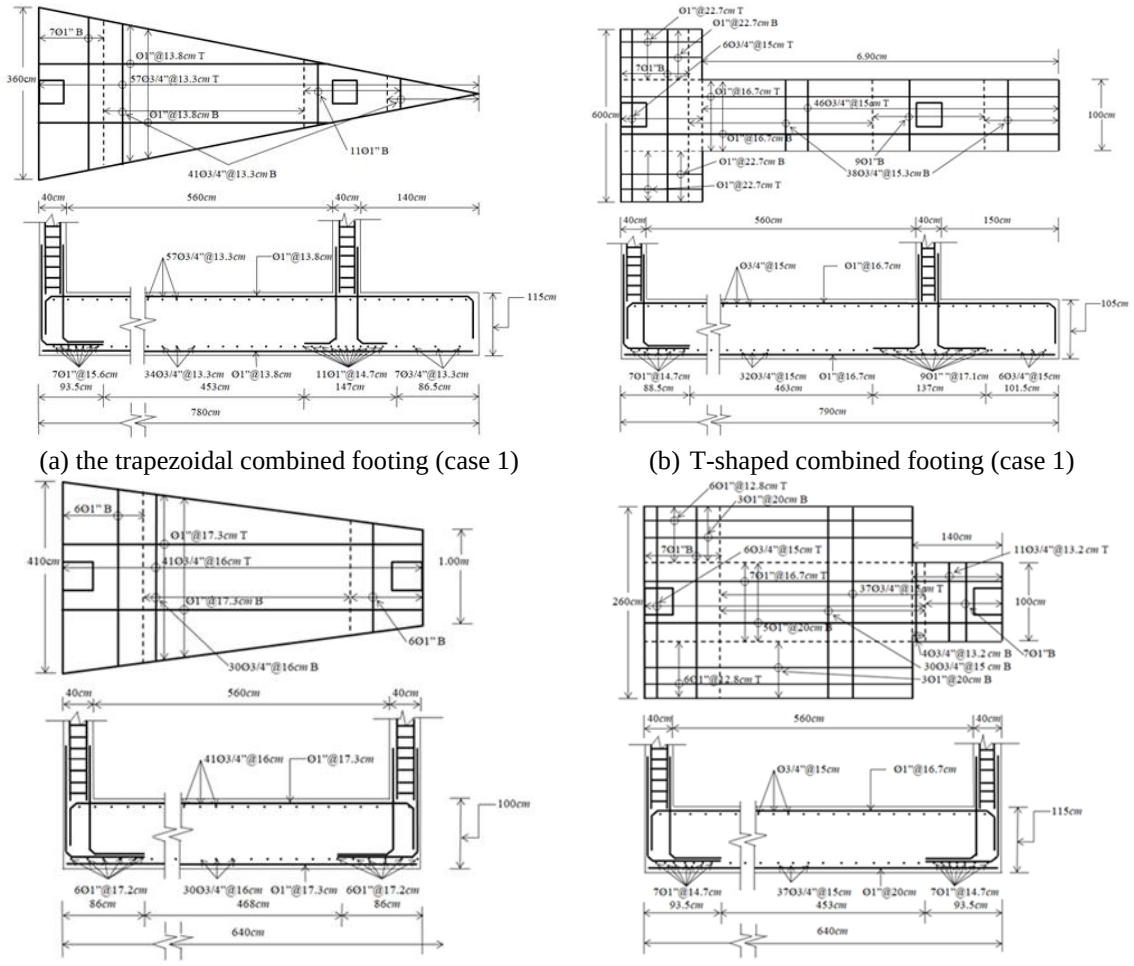

(a) the trapezoidal combined footing (case 1) (b) T-shaped combined footing (case 1)

(c) the trapezoidal combined footing (case 2) (d) T-shaped combined footing (case 2)

Fig. 10 Final design for the four footings

resists the concrete for the two cases and the two footings, and the value that governs is the lowest (ACI 318-14).

Fig. 10 shows the sides and the reinforcing steel for the two cases and the two footings.

4. Results

Table 6 shows the comparison of the dimensions for the trapezoidal combined footings and the T-shaped combined footings.

Table 7 shows the comparison of the volumes of concrete and steel for the trapezoidal combined footings and the T-shaped combined footings.

The results show the following:

The critical bending shear: The critical bending shear is located on the *h'-h'* axis for the cases 1 and 2 of the trapezoidal combined footings, and for the T-shaped combined footings is located on the *l*'-*l*' axis for the case 1 and for the case 2 is located on the *k*'-*k*' axis (see Table 4).

The dimensions: The area of the contact surface of the footing on the soil is less for the T-shaped combined footings in the two cases (see Table 6). The effective depth and thickness of the footing is less for the T-shaped combined footing in case 1 and for the case 2 is less for the trapezoidal combined footing (see Table 6).

The volumes of concrete and steel: The volume of concrete for the footing is less for the T-shaped combined footing in case 1 and for el case 2 is less for the trapezoidal combined footing (see Table 7). The volume of steel for the footing is less for the trapezoidal combined footing in case 1 and for el case 2 is less for the T-shaped combined footing (see Table 7).

To make a decision on the most economical footing, the total cost must be considered.

The total cost "C_t" for any type of footing is:

Table 6 Comparison of the dimensions

Concept	TCF		T-SCF		TCF_1/T-SCF_1	TCF_2/T-SCF_2
Case	1	2	1	2		
A_t (m^2)	14.04	16.32	12.90	14.40	1.09	1.13
d (cm)	107	92	97	107	1.10	0.86
r (cm)	8	8	8	8	1	1
t (cm)	115	100	105	115	1.10	0.91

where: TCF=Trapezoidal combined footings, T-SCF=T-shaped combined footings, TCF_1=Trapezoidal combined footings for case 1, T-SCF_1=T-shaped combined footings for case 1, TCF_2=Trapezoidal combined footings for case 2, T-SCF_2=T-shaped combined footings for case 2

Table 7 Comparison of the volumes

Concept	TCF		T-SCF		TCF_1/T-SCF_1	TCF_2/T-SCF_2
Case	1	2	1	2		
V_c (m^3)	16.15	16.32	13.54	16.56	1.19	0.99
V_s (m^3)	0.1589	0.1595	0.1713	0.1516	0.93	1.05

where: V_c=Volume of concrete, V_s=Volume of steel

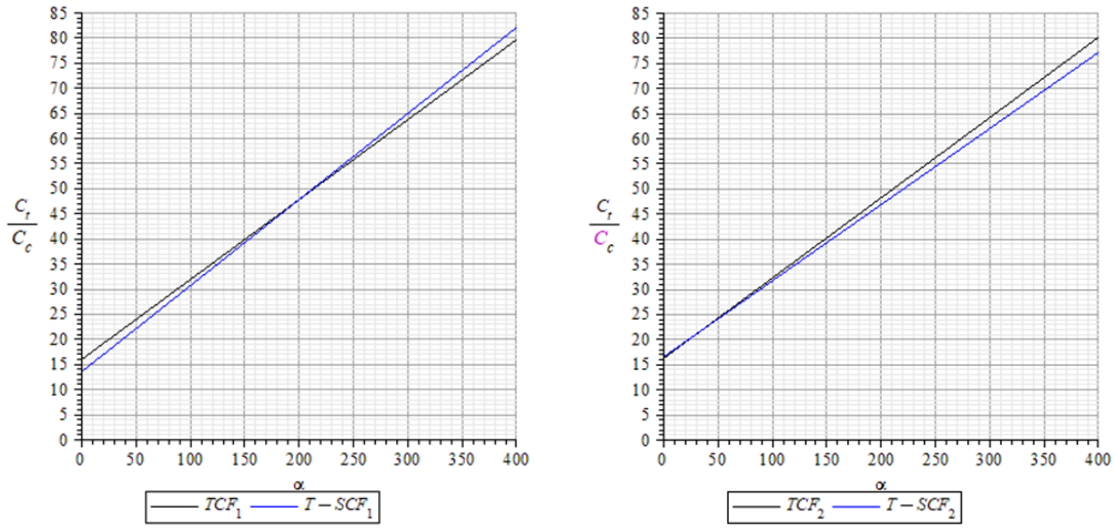

(a) Case 1 (b) Case 2

Fig. 11 Comparison of the total cost for the two footings

$$C_t = V_c C_c + V_s \gamma_s C_s \tag{78}$$

where: C_c=cost of concrete for 1 m^3 of ready-mix reinforced concrete in dollars, C_s=cost of reinforcing steel for 1 kN of steel in dollars, V_s=volume of reinforcing steel, V_c=volume of concrete, and γ_s=steel density=76.94 kN/m^3.

Substituting α=ratio of reinforcement steel cost to concrete cost=$\gamma_s C_s/C_c \rightarrow \gamma_s C_s = \alpha C_c$ into Eq. (78) is presented by the following equation

$$C_t = (V_c + \alpha V_s) C_c \tag{79}$$

Fig. 11 shows the graphics of the relationship between the total cost and the concrete cost in function of α of the trapezoidal combined footing and the T-shaped combined footing for the two cases.

Fig. 11(a) shows the graphics for the case 1, where the relationship between the total cost and the concrete cost is greater for the trapezoidal combined footing until α=210.48, and from this value, the relationship is greater for the T-shaped combined footing.

Fig. 11(b) shows the graphics for the case 2, where the relationship between the total cost and the concrete cost is greater for the T-shaped combined footing until α=30.48, and from this value, the relationship is greater for the trapezoidal combined footing.

5. Conclusions

Foundation of a structure is the essential part to transmit the column or wall loads to the underlying ground below the structure. The comparative study between trapezoidal and T-shaped combined footings presented in this paper generates results that have an unparalleled accuracy for all foundation engineering problems. The main part of this research is to obtain the optimal area, reinforcing steel and thickness of the trapezoidal and T-shaped combined footings using the new

models.

This study assumes that soil support layers are elastic and the rigid footing, which comply with the biaxial bending equation, i.e., the pressure diagram presents a linear variation.

The advantages of the two models presented in this document are:

1) The models can be used for different types of loads and moments such as: P_1, P_2, M_{x1}, M_{y1}, M_{x2}, and M_{y2}.

2) The models can be used for different types of allowable load capacity of the soil "q_a",

3) The moments and bending shear can be obtained anywhere on the footing, because the equations are presented in function of the variable "y",

The proposed model presented in this article can be applied to the following types:

1) Footings under concentric load in each column.

2) Footings under concentric load and moment in a direction in each column.

3) Footings under concentric load and moments in both directions in each column.

The main conclusions are:

1. The classical model will not be practical compared to this methodology; because the classical model takes into account only the greater pressure applied throughout the contact surface of the footing (pressure is equal in all points of the footing).
2. The new model for the design of trapezoidal combined footings can be used:
   2.1. For the design of trapezoidal combined footings with a property line restricted, and also two property lines of opposite sides restricted.
   2.2. For the design of triangular combined footings with a restricted property line considering b_2=0 (see case 1).
   2.3. For the design of rectangular combined footings with a restricted property line considering b_1=b_2, and also two property lines of opposite sides restricted.
3. The new model for the design of T-shaped combined footings can be used:
   3.1. For the design of T-shaped combined footings with a property line restricted, and also two property lines of opposite sides restricted.
   3.2. For the design of rectangular combined footings with a restricted property line considering b=b_1 and a=b_2, and also two property lines of opposite sides restricted.
4. The optimal area for T-shaped combined footings are more economical than the trapezoidal combined footings as seen in the results section (see Table 6).

Suggestions for next investigations can be:

1.- If there is another type of soil, such as totally clayey soils (cohesive soils) or totally sandy soils (granular soils), the pressure diagram should be considered differently because it is not linear.

2.- Comparative study of T-shaped combined footings between the model proposed in this paper and any other type of finite element software to observe the results.

3.- Comparative study of trapezoidal combined footings between the model proposed in this work and any other type of finite element software to observe the results.

References

ACI 318-14 (American Concrete Institute) (2014), Building Code Requirements for Structural Concrete and Commentary, Committee 318.

Al-Abbas, K.A., Saadoon, S. and Al-Robay, A.A. (2020), "Experimental study for elastic deformation under isolated footing", *Period. Eng. Nat. Sci.*, **8**(2), 942-948. https://doi.org/10.21533/PEN.V8I2.1353.G577.

Anil, O., Akbas, S.O., Babaglray, S., Gel, A.C. and Durucan, C. (2017), "Experimental and finite element analyses of footings of varying shapes on sand", *Geomech. Eng.*, **12**(2), 223-238. http://doi.org/10.12989/gae.2017.12.2.223.

Chen, W.R., Chen, C.S and Yu, S.Y. (2011), "Nonlinear vibration of hybrid composite plates on elastic foundations", *Struct. Eng. Mech.*, **37**(4), 367-383. http://doi.org/10.12989/sem.2011.37.4.367.

Dagdeviren, U. (2016), "Shear stresses below the rectangular foundations subjected to biaxial bending", *Geomech. Eng.*, **10**(2), 189-205. http://doi.org/10.12989/gae.2016.10.2.189.

Gandomi, A.H. and Kashani, A.R. (2018), "Construction cost minimization of shallow foundation using recent swarm intelligence techniques", *IEEE Trans. Indus. Inform.*, **14**(3), 1009-1106. https://doi.org/10.1109/TII.2017.2776132.

Guler, K. and Celep, Z. (2005), "Response of a rectangular plate-column system on a tensionless Winkler foundation subjected to static and dynamic loads", *Struct. Eng. Mech.*, **21**(6), 699-712. https://doi.org/10.12989/sem.2005.21.6.699.

Hadzalic, E., Ibrahimbegovic, A. and Dolarevic, S. (2018), "Fluid-structure interaction system predicting both internal pore pressure and outside hydrodynamic pressure", *Couple. Syst. Mech.*, **7**(6), 649-668. https://doi.org/10.12989/csm.2018.7.6.649.

Hadzalic, E., Ibrahimbegovic, A. and Dolarevic, S. (2020), "3D thermo-hydro-mechanical coupled discrete beam lattice model of saturated poro-plastic medium", *Couple. Syst. Mech.*, **9**(2), 125-145. https://doi.org/10.12989/csm.2020.9.2.125.

Hassaan, G.A. (2014), "Optimal design of machinery shallow foundations with sand soils", *Int. J. Res. Eng. Technol.*, **3**(5), 1-8.

Ibrahimbegovic, A. and Mejia-Nava, R.A. (2021), "Heterogeneities and material-scales providing physicallybased damping to replace Rayleigh damping for any structure size", *Couple. Syst. Mech.*, **10**(3), 201-216. https://doi.org/10.12989/csm.2021.10.3.201.

Khajehzadeh, M., Taha, M.R., El-Shafie, A. and Eslami, M. (2012), "Optimization of shallow foundation using gravitational search algorithm", *Res. J. Appl. Sci. Eng. Technol.*, **4**(9). 1124-1130.

Khatri, V.N., Debbarma, S.P., Dutta, R.K. and Mohanty, B. (2017), "Pressure-settlement behavior of square and rectangular skirted footings resting on sand", *Geomech. Eng.*, **12**(4), 689-705. https://doi.org/10.12989/gae.2017.12.4.689.

López-Chavarría, S., Luévanos-Rojas, A. and Medina-Elizondo, M. (2017), "Optimal dimensioning for the corner combined footings", *Adv. Comput. Des.*, **2**(2), 169-183. https://doi.org/10.12989/acd.2017.2.2.169.

Luat, N.V., Lee, K. and Thai, D.K. (2020), "Application of artificial neural networks in settlement prediction of shallow foundations on sandy soils", *Geomech. Eng.*, **20**(5), 385-397. https://doi.org/10.12989/gae.2020.20.5.385.

Luévanos-Rojas, A. (2014), "Design of boundary combined footings of rectangular shape using a new model", *Dyn.*, **81**(180), 199-208. https://doi.org/10.15446/dyna.v81n188.41800.

Luévanos-Rojas, A. (2015a), "A New Mathematical Model for Dimensioning of the Boundary Trapezoidal Combined Footings", *Int. J. Innov. Comput. I.*, **11**(4), 1269-1279.

Luévanos-Rojas, A. (2015b), "Design of boundary combined footings of trapezoidal form using a new model", *Struct. Eng. Mech.*, **56**(5), 745-765. http://doi.org/10.12989/sem.2015.56.5.745.

Luévanos-Rojas, A. (2016), "A comparative study for the design of rectangular and circular isolated footings using new models", *Dyn.*, **83**(196), 149-158. https://doi.org/10.15446/dyna.v83n196.51056.

Luévanos-Rojas, A., Barquero-Cabrero, J.D., López-Chavarría, S. and Medina-Elizondo, M. (2017b), "A comparative study for design of boundary combined footings of trapezoidal and rectangular forms using new models", *Couple. Syst. Mech.*, **6**(4), 417-437. https://doi.org/10.12989/csm.2017.6.4.417.

Luévanos-Rojas, A., López-Chavarría, S. and Medina-Elizondo, M. (2017a), "Optimal design for rectangular isolated footings using the real soil pressure", *Ing. Invest.*, **37**(2), 25-33. https://doi.org/10.15446/ing.investig.v37n2.61447.

Luévanos-Rojas, A., López-Chavarría, S. and Medina-Elizondo, M. (2018a), "A new model for T-shaped combined footings Part I: Optimal dimensioning", *Geomech. Eng.*, **14**(1), 51-60. https://doi.org/10.12989/gae.2018.14.1.051.

Luévanos-Rojas, A., López-Chavarría, S. and Medina-Elizondo, M. (2018b), "A new model for T-shaped combined footings Part II: Mathematical model for design", *Geomech. Eng*., **14**(1), 61-69. https://doi.org/10.12989/gae.2018.14.1.061.

Maheshwari, P. (2017), "Analysis of combined footings on extensible geosynthetic-stone column improved ground", *J. Civil Eng., Sci. Technol.*, **8**(2), 57-71. https://doi.org/10.33736/JCEST.439.2017.

Maheshwari, P. and Khatri, S. (2012), "Influence of inclusion of geosynthetic layer on response of combined footings on stone column reinforced earth beds", *Geomech. Eng*., **4**(4), 263-279. https://doi.org/10.12989/gae.2012.4.4.263.

Mejia-Nava, R.A., Ibrahimbegovic, A., Domínguez-Ramírez, N. and Flores-Méndez, E. (2021), "Viscoelastic behavior of concrete structures subject to earthquake", *Couple. Syst. Mech.*, **10**(3), 263-280. https://doi.org/10.12989/csm.2021.10.3.263.

Mohamed, F.M.O., Vanapalli, S.K. and Saatcioglu, M. (2013), "Generalized Schmertmann Equation for settlement estimation of shallow footings in saturated and unsaturated sands", *Geomech. Eng*., **5**(4), 363-377. https://doi.org/10.12989/gae.2013.5.4.343.

Mohebkhah, A. (2017), "Bearing capacity of strip footings on a stone masonry trench in clay", *Geomech. Eng.*, **13**(2), 255-267. https://doi.org/10.12989/gae.2017.13.2.255.

Orbanich, C.J. and Ortega, N.F. (2013), "Analysis of elastic foundation plates with internal and perimetric stiffening beams on elastic foundations by using Finite Differences Method", *Struct. Eng. Mech.*, **45**(2), 169-182. https://doi.org/10.12989/sem.2013.45.2.169.

Orbanich, C.J., Dominguez, P.N. and Ortega, N.F. (2012), "Strenghtening and repair of concrete foundation beams whit fiber composite materials", *Mater. Struct.*, **45**, 1693-1704. http://dx.doi.org/10.1617/s11527-012-9866-6.

Rad, A.B. (2012), "Static response of 2-D functionally graded circular plate with gradient thickness and elastic foundations to compound loads", *Struct. Eng. Mech*., **44**(2), 139-161. https://doi.org/10.12989/sem.2012.44.2.139.

Rawat, S. and Mittal, R.K. (2018), "Optimization of eccentrically loaded reinforced-concrete isolated footings", *Pract. Period. Struct. Des. Constr.*, **23**(2). 06018002. https://doi.org/10.1061/(ASCE)SC.1943-5576.0000366.

Rezaei, H., Nazir, R. and Momeni, E. (2016), "Bearing capacity of thin-walled shallow foundations: an experimental and artificial intelligence-based study", *J. Zhejiang Univ.-Sci. A (Appl. Phys. Eng.)*, **7**(4), 273-285.

Sahoo, J.P. and Kumar, J. (2015), "Ultimate bearing capacity of shallow strip and circular foundations by using limit analysis, finite elements, and optimization", *Int. J. Geotech. Eng.*, **9**(1), 30-41. https://doi.org/10.1179/1939787914Y.0000000070.

Shahin M.A. and Cheung E.M. (2011), "Stochastic design charts for bearing capacity of strip footings", *Geomech. Eng*., **3**(2), 153-167. http://doi.org/10.12989/gae.2011.3.2.153.

Smith-Pardo, J.P. (2011), "Performance-based framework for soil-structure systems using simplified rocking foundation models", *Struct. Eng. Mech.*, **40**(6), 763-782. http://doi.org/10.12989/sem.2011.40.6.763.

Turedi, Y., Emirler, B., Ornek, M. and Yildiz, A. (2019), "Determination of the bearing capacity of model ring footings: Experimental and numerical investigations", *Geomech. Eng*., **18**(1), 29-39. http://doi.org/10.12989/gae.2019.18.1.029.

Uncuoğlu, E. (2015), "The bearing capacity of square footings on a sand layer overlying clay", *Geomech. Eng.*, **9**(3), 287-311. http://doi.org/10.12989/gae.2015.9.3.287.

Wang, Y. and Kulhawy, F.H. (2008), "Economic design optimization of foundations", *J. Geotech. Geoenviron. Eng.*, **134**(8), 1097-1105. https://doi.org/10.1061/(ASCE)1090-0241(2008)134:8(1097).

Zhang, W.X. Wu, H., Hwang, H.J., Zhang, J.Y., Chen, B. and Yi, W.J. (2019), "Bearing behavior of reinforced concrete column-isolated footing substructures", *Eng. Struct.*, **200**, 109744. https://doi.org/10.1016/j.engstruct.2019.109744.